MATERIALS SCIENCE

MycelioTronics: Fungal mycelium skin for sustainable electronics

Doris Danninger[1,2]†, Roland Pruckner[1,2]†, Laura Holzinger[3], Robert Koeppe[1,4], Martin Kaltenbrunner[1,2]*

Electronic devices are irrevocably integrated into our lives. Yet, their limited lifetime and often improvident disposal demands sustainable concepts to realize a green electronic future. Research must shift its focus on substituting nondegradable and difficult-to-recycle materials to allow either biodegradation or facile recycling of electronic devices. Here, we demonstrate a concept for growth and processing of fungal mycelium skins as biodegradable substrate material for sustainable electronics. The skins allow common electronic processing techniques including physical vapor deposition and laser patterning for electronic traces with conductivities as high as 9.75 ± 1.44 × 10^4 S cm^{-1}. The conformal and flexible electronic mycelium skins withstand more than 2000 bending cycles and can be folded several times with only moderate resistance increase. We demonstrate mycelium batteries with capacities as high as ~3.8 mAh cm^{-2} used to power autonomous sensing devices including a Bluetooth module and humidity and proximity sensor.

INTRODUCTION

Wearable and untethered electronics are increasingly accessible to various fields, with applications ranging from robotics to medical applications and consumer electronics (*1*–*3*). The vast number of devices produced every day along with the decrease of their lifetime inevitably results in the generation of enormous amounts of electronic waste (*4*). Circular economy and recycling concepts alone cannot solve the growing waste crisis. Electronics research, and especially electronic materials research, thus must shift its focus from strictly high-functionality concepts to sustainable, cost-effective approaches (*5*, *6*). Wearable devices are designed to function in close interaction with their user, combining conventional electronics such as transistors with sensors allowing the collection of a plethora of signals (*7*). Fabricating such smart devices with sustainable materials, however, is still a challenge. Carbon biomaterials including carbon nanotubes and graphene are promising due to their excellent electronic and mechanical characteristics and may lead to a new class of electronics, yet the majority of reported devices still incorporate unsustainable substrates (*8*–*11*). Li *et al.* (*12*), for instance, not only demonstrate carbonized cotton sensors with good sensing performance but also include the silicone-based elastomer polydimethylsiloxane in their composite. However, to realize truly sustainable electronics, every component of a device must be substituted with environmentally benign alternatives. Integrated circuits (ICs) make up the majority of the total mass of printed circuit boards (PCBs), due to the high density of the metals used, yet biodegradable versions of such are difficult to realize. Conventional PCBs of mobile phones, for instance, consist of 63 weight % (wt %) metals, 24 wt % ceramics, and 13 wt % polymers (*13*). Reported works on biodegradable ICs are based on biomass and plant-based materials, yielding entirely transient electronics including degradable circuit elements (*14*, *15*). These, although promising, exhibit still limited performance, durability, and, hence, applicability. With the substrate being the second major contributor to the total mass of a PCB (37 wt %), developing biodegradable alternatives of such serves as a viable route for sustainable electronics (*13*, *16*). By combining conventional (eventually reusable) ICs with a biodegradable substrate instead of hard to recycle polymers and plastics, e-waste can already be reduced markedly. Flexible PCBs on paper substrates demonstrate the feasibility of combining nondegradable IC components with a new class of substrates (*17*–*19*). Cellulose nanofibril paper allows processing of sophisticated electronics as, for example, gallium arsenide microwave devices on its surface (*20*, *21*). However, the production process of paper is resource intensive, requiring, on average, 300 million liters of water and 33.76 GJ energy per ton and involves the use of large amounts of toxic acids, solvents, and bases in the process (*22*). We herein propose a new electronic substrate material as an alternative, a fungal mycelium "skin" based on a saprophytic fungus *Ganoderma lucidum* growing naturally on dead hardwood in mild temperate climates (Fig. 1A) (*23*, *24*). We report on a method for its efficient and scalable growth and harvest and its use in a new approach toward flexible and biodegradable electronics called MycelioTronics. Pure fungus mycelium exhibits promising properties, closer to high-performance polymer microfoams than to other as-grown biomaterials, and environmentally benign post-treatment procedures allow tuning of mechanical properties (*25*, *26*). Our material, being entirely biodegradable, therefore renders the replacement of fossil-based and heavily processed components of electronics feasible (*27*). We couple our fungus material with conventional nondegradable circuit components, achieving high-functionality electronic devices without sacrificing sustainability (Fig. 1B). To date, combinations of fungus mycelium with electronics and sensing platforms are scarce. Recent developments in this field are either unfavorably bulky or exhibit limited sensing performance (*28*, *29*). We demonstrate the fabrication of lightweight and shape-adaptive standalone sensor patches based on an as-grown fungus mycelium substrate and highlight general processing techniques of mycelium skin for electronics. We construct conductor paths by metalizing mycelium surfaces via physical vapor

[1]Division of Soft Matter Physics, Institute for Experimental Physics, Johannes Kepler University, Altenberger Str. 69, Linz 4040, Austria. [2]Soft Materials Lab, Linz Institute of Technology, Johannes Kepler University, Altenberger Str. 69, Linz 4040, Austria. [3]Institute of Polymer Science, Johannes Kepler University, Altenberger Str. 69, Linz 4040, Austria. [4]Sendance GmbH, Pulvermühlstr. 3, Linz A-4040, Austria.
*Corresponding author. Email: martin.kaltenbrunner@jku.at
†These authors contributed equally to this work.

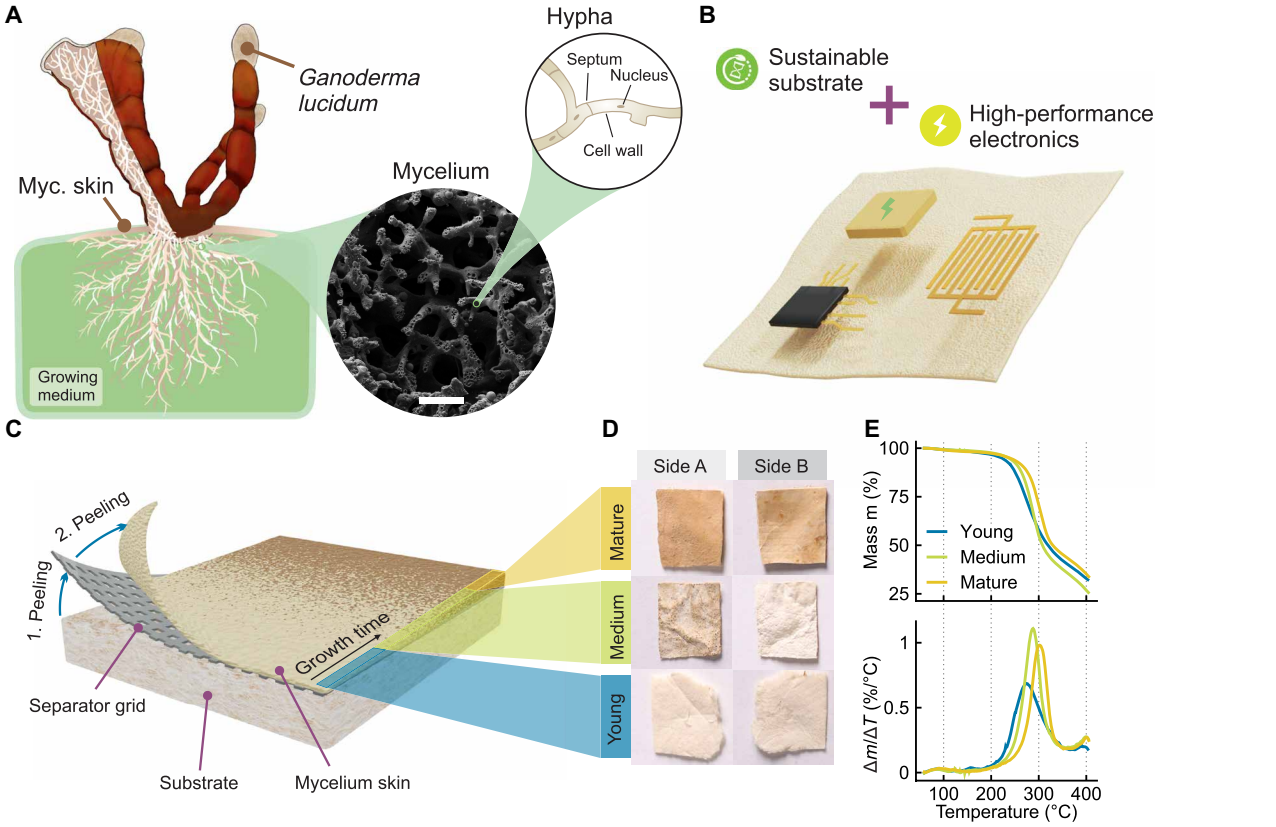

Fig. 1. Formation and properties of mycelium skin. (**A**) Structure of *G. lucidum* fungus. Mycelium roots are growing inside the chosen medium, with fruiting bodies forming on the surface at longer growth times. Mycelium strains consist of hyphen structures on a microscopic level. Scale, bar 10 μm. (**B**) Concept of using mycelium skin as substrate for electronic devices. (**C**) Growth of mycelium skin on PE-separator grid and underlying substrate. (**D**) Three distinct types of mycelium skin are obtained depending on the growth time. Sides A and B refer to the surface in contact with the surrounding air and the separation grid, respectively. (**E**) TGA of all mycelium types with a constant temperature change of 0.166 K/s, revealing thermal stability to more than 250°C.

deposition (PVD) of thin metal layers and subsequent laser ablation. Our mycelium skin exhibits high thermal stability, allowing soldering of electronic components and facilitating the fabrication of electronic sensor boards, not restricted to planar geometry due to its shape adaptiveness. In addition, we propose a new concept of mycelium batteries, using our skins both as battery separators and casing. We achieve untethered operation of a standalone circuit directly incorporating our mycelium battery, a capacitive sensor, and all necessary communication modules. We demonstrate the versatility of the material for sustainable electronics on a profound level, bringing us closer toward a more sustainable architecture of electronic devices.

RESULTS

Mycelium skin growth, harvest, and characterization

We fabricate our mycelium skins by covering moist beech wood–based inocula with a polyethylene (PE) separation grid and storing them at 25°C (details given in Materials and Methods). The humid and CO_2-rich atmosphere allows the growth of *G. lucidum* fungus and the formation of mycelium skins on the surface. Its development on the surface exhibits three distinct phases (Fig. 1C and fig. S1). During the first phase ("young" skin), the surface has a bright white color while covering the separation grid with an increasingly dense layer (Fig. 1D). In the second phase ("medium" skin), the skin grows more thick and dense, and brown patches appear on the surface that are covered with a rough crust. The third phase ("mature" skin) is marked by a complete coverage of the surface with the brown crust. Thereafter, the skin formation is complete, and the growth process stops. We observe growth times to be approximately 2 weeks until a closed sheet of young skin is formed and two further weeks until it can be classified as mature. Further optimizing the starting and growth conditions could potentially accelerate and stabilize this process substantially. Moreover, primordia formation and subsequently the formation of fruiting bodies must be suppressed to obtain a smooth skin. Thus, exposure to light must be minimized, and a high level of CO_2 in the surrounding atmosphere must be maintained. Directly after the harvest, the skins are composed of living mycelium, saturated with water, thus we impose additional compressing and drying, yielding the final skins. Hereby, the grammage of the skins is reduced by up to a factor of 8, and we observe slight shrinking (<10%) and notable stiffening (fig. S2C). Our growth and harvest method is readily scalable to yield areas of several square meters, depending mostly on the growing substrate. Irregular growth, the malleable material with soft and fuzzy surfaces, and inhomogeneities in the pressing and drying process result in variations in skin thickness over the harvested area (table S1). Thus, sample grammage is more suitable to characterize larger areas of our mycelium skin. Furthermore, our substrate is able to supply nutrients for

additional skin growth, enabling several mycelium skin harvests all from one source material. We achieved a maximum of five subsequent harvests from one growing medium over a period of 6 weeks with sufficient yield and quality of the obtained mycelium skins. To achieve such high growth cycle numbers, we prevent contamination of the surface and the separation grid with competing organisms by maintaining a high level of cleanliness, as contamination may lead to irregular skin formation. Growth of the fungus can be terminally stopped after harvest by drying and heating the remaining biodegradable mycelium-beech wood composite. The remainder exhibits low density and comparatively high compressive and tensile strength due to the long growth time. These properties render it suitable to be further used in various applications such as mycelium composite construction or packaging (*30*). Alternatively, the fungus can as well still produce a certain amount of fruiting bodies for medical purposes from the remaining substrate block. Utilization of abundant agricultural waste to obtain multiple high-value products, as proposed in our method, is an indispensable aspect of sustainable fabrication routes and conforms perfectly with proposed schemes for biorefineries in a circular economy (*31*–*33*). To allow combination of our substrate with standard electronic processing techniques, a high temperature stability is indispensable. Thermogravimetric analysis (TGA) (Fig. 1E) of all three skin types in pure oxygen atmosphere demonstrates the material stability up to more than 250°C, with the critical temperature increasing slightly with the age of the skin. This allows processing of electrical components on top of our substrate using standard techniques like soldering.

Electronic circuits on mycelium skin

The excellent thermal stability and electrically insulating nature of the hyphen network renders our mycelium skin a highly suitable biodegradable substrate for electronic circuit boards. We herein demonstrate several routes for functionalization, forming the foundation for further use in electronic circuits and sensor technology (Fig. 2A). We achieve cohesive metallic films on top of harvested skins with a surface roughness R_{rms} of 7.5 ± 1.8 μm by PVD (fig. S3), which allow for further processing to circuit paths. We obtain films with reproducible continuity by depositing 400 nm of copper as conductive bulk, with predeposition of 3 nm of chromium for better adhesion (Fig. 2B) (*34*). We further improve conductivity by depositing an additional layer of gold with a thickness of 50 nm onto the initial copper layer. As an alternative route, we demonstrate gold plating of the already metalized (copper) mycelium, using electroplating and a respective electrolyte solution. For this purpose, metalized mycelium is dipped into the plating solution along with a stainless-steel anode, both connected to a power supply, with the plating process then being controlled by the applied current. Our metalized mycelium skin hence enables the fabrication of traces and pads for electronic circuit boards in an easily scalable manner. The additional gold coating is especially advantageous at connecting pads and soldering points, where copper corrosion would otherwise diminish performance. We then pattern conductive traces into our mycelium-metal films by laser ablation, without impairing the mechanical integrity of the underlying substrate (Fig. 2C and fig. S2). Trace conductivity decreases with increasing skin age, as the surface structure changes in the growth process (Fig. 2D). We achieve a high trace conductivity of 9.75 ± 1.44 × 10^4 S cm^{-1} with the bulk-facing side of young skin, comparable with conductors on common printing paper (*17*, *35*). In general, the electrical properties of young mycelium are similar to paper-based substrates (*18*, *35*); they exhibit a breakdown strength of 13.5 ± 3.7 kV mm^{-1}, a relative permittivity of ε_r = 3 ± 0.9, a loss tangent of δ = 0.06 ± 0.01 at 1 MHz, and a conductivity of 0.27 ± 0.1 μS m^{-1} at 10 MHz (see fig. S4 for details). With increasing skin maturity, formation of islands of rough crusts disrupts the continuity of the surface, hence impairing the formation of continuous metal films. Consequently, side B exhibits higher conductivity values across all ages, as little to no crust forms on the side facing the bulk growing medium opposed to side A, which is in contact with the surrounding air. For mature mycelium skin with a fully developed crust, no continuous metal film could be formed. With this insight, we focus all following demonstrations on the bulk side of young mycelium. Traces fabricated using this approach can sustain high current densities up to 333 A mm^{-2}, before electrode failures due to overheating arise (figs. S5 and S6). In addition to its high conductivity, the lack of crust and overall low thickness yield high flexibility of the fabricated traces. Cyclic bending of a single Cu-Au trace between a bending radius of 22.5 and 5 mm is feasible for more than 2000 bending cycles with only a small increase in resistance of 18.1% (Fig. 2E). We observe a burn-in effect in the first cycles, wherein the resistance increases by 6% in the first 10 cycles. In later iterations, the resistance changes only marginally within 1 cycle indicating only minimal damage of hyphen connections (Fig. 2F). At around 2000 cycles, the metal film begins to crack over larger areas with each cycle, resulting in a steep resistance increase (fig. S7), similarly to the behavior observed in metal depositions on plain polymer substrates (*36*). We achieve not only bending of metallic traces but also folding of metalized mycelium several times is feasible while remaining fully functional (Fig. 2G and fig. S8). The normalized resistance R/R_0 rises to 4.07 ± 0.51 after imposing 12-fold (Fig. 2H), comparable to reports on glossy printing papers with substantially lower surface roughness (*17*). The ability of our metalized mycelium skin to withstand such extreme deformations with reasonable increases in resistance thus allows the realization of complex conductor geometries. Surface mounting of electronics to passive components can be imposed onto MycelioTronic devices without major performance losses under deformation. Our mycelium skins can be permanently forced into numerous geometries by exploiting the soakability of the foam-like hyphen network using a hydrosetting method (*37*). Soaking the mycelium with 2-propanol, subsequently reshaping it into its desired form using a mold (fig. S9), and lastly air drying of the skin in ambient environment in its deformed state yield a permanently deformed yet fully functional MycelioTronic device. To illustrate this concept of shape-adaptive electronics, we reshape a conductor strip including a surface mounted device–light-emitting diode (SMD-LED) into a helical structure, with the LED's luminosity not being visibly diminished (Fig. 2I). Such MycelioTronic devices can further be encapsulated using a biodegradable shellac-ethanol varnish to ensure electrical insulation and be used for wearable applications as well (fig. S10).

Mycelium skin for flexible and biodegradable batteries

Our mycelium skin cannot only be used as a substrate for sustainable electronic circuits. With its highly porous structure, mycelium skin can soak up large amounts of liquid and is thus a promising candidate for realizing sustainable battery separators (fig. S11). Electronic devices rely heavily on either external or integrated power sources, with truly sustainable solutions being scarce. Larcher *et al.* (*38*), for example, discuss the importance of developing greener battery

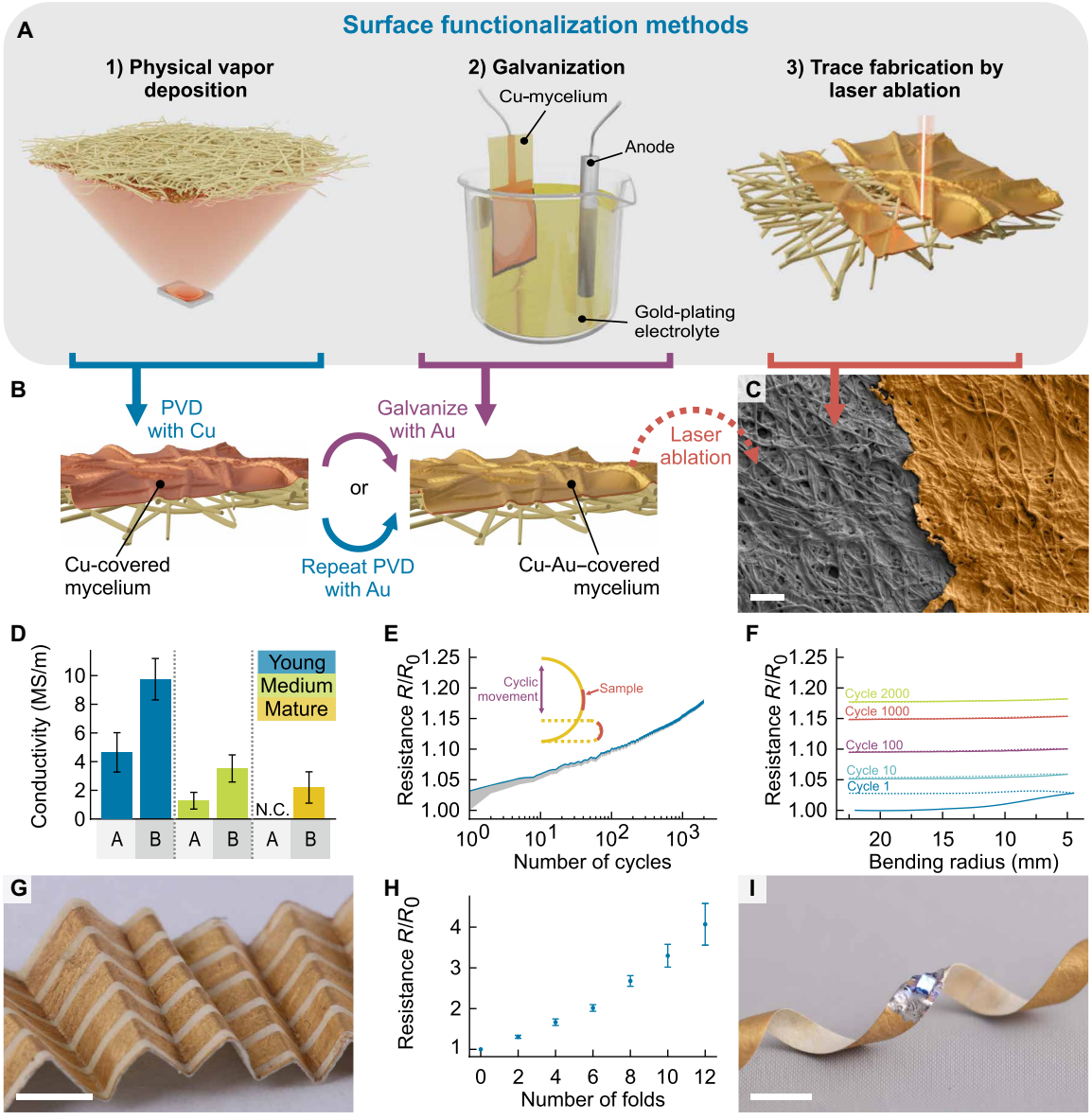

Fig. 2. Functionalization methods for mycelium skin. (**A**) Possible functionalization methods of mycelium skin. (**B**) Formation of Cu and Cu-Au bilayer films on mycelium skin. (**C**) Colorized SEM image of a laser-ablated edge of a Cu-Au layer fabricated by PVD (3 nm of Cr, 400 nm of Cu, and 50 nm of Au) on a young mycelium skin (side A). Scale bar, 20 μm. (**D**) Conductivity of a PVD-Cu-Au layer on young, medium, and mature mycelium skin, sides A and B. $n = 5$. N.C., non-conducting. (**E**) Normalized resistance of young Cu-Au–covered mycelium during cyclic bending over 2000 times between bending radii of 5 and 25 mm. Variation of resistance in 1 cycle (gray) decreases with the number of cycles, while the maximum (blue) increases. (**F**) Normalized resistance of selected cycles of (E) as a function of bending radius. (**G**) Optical image of Cu-Au traces on a young mycelium skin after recovery of several hard folds being imposed. Scale bar, 5 mm. (**H**) Normalized resistance of conductor traces increases with the number of applied folds. $n = 5$. (**I**) Photograph of a young mycelium skin conductor strip with a surface mounted LED reshaped into a helix. Scale bar, 5 mm.

chemistries in detail. Thus, we herein are focusing on demonstrating sustainable concepts for the passive components and building blocks of a battery, universal and not restricted to battery chemistry, namely, the separator and packaging. With this approach, we substitute the bulk volume of a typical battery with a sustainable material. Yet, depending on the battery chemistry, different requirements must be met by a material to be suitable as a separator. Commercial Li-ion batteries mostly use polyolefin polymer separators, as they exhibit excellent mechanical properties, are chemically stable with respect to lithium chemistries, and can be produced with small enough pore sizes to incorporate safety mechanisms (*39*). However, these are nonrenewable petroleum products, both expensive and unfavorable in terms of environmental impact. The use of biomaterials as battery separators is still very limited and must increase for a transition to more and more sustainable portable energy sources (*40*). Mycelium skin separators may serve as an eco-friendly alternative, as they can be grown naturally and consume little resources even compared to paper-based materials (*41*). We herein use the mycelium skin's

ability to soak up high amounts of liquid in combination with a highly ion-conducting electrolyte solution, yielding a flexible membrane that can be readily incorporated in batteries as separator material. We test their performance using primary zinc-carbon cell chemistry, using a conventional ammonium chloride and zinc chloride solution as electrolyte (Fig. 3A). The solution fills the cavities of the otherwise dry sheets of mycelium skin by soaking for 12 hours. We determine the quality of ion transport through the bulk material by impedance spectroscopy of the liquid-filled separators using a custom-built measurement cell (*42*). Mycelium skin of type medium exhibits the lowest specific resistance (Fig. 3B), being as low as 54.3 ± 19.8 ohm cm with our electrolyte solution, rendering it a viable separator material. However, the ability to transport ions is inevitably lowered by any separator material when compared to unrestrained, i.e., freestanding liquid electrolyte solutions. Conductivity itself highly depends on the used electrolyte solution and is hence not universal with respect to the used chemistry. To ease comparison with other materials, the quality of a separator is also described by the MacMullin number, being the ratio between freestanding electrolyte conductivity and separator conductivity. With medium mycelium skin, we achieve MacMullin numbers as low as 6.7, making them comparable to commercial Li-ion battery separators in this respect (*39*). In the construction of full cells, mycelium skin does not only serve as a well-conducting separator, we also use the same material in its dry form as packaging. Thus, we are already substituting many components of a standard zinc-carbon cell with a sustainable alternative, making a high percentage of the resulting battery biocompatible and biodegradable (Fig. 3C). In our demonstration, electrode materials are constructed as pastes, with the anode being a zinc paste, and the cathode being a manganese dioxide and carbon black paste. The outer packaging layers are mycelium skin foils metalized on one side, to allow collection of the current generated by the battery. For the cathode current collector, both vapor-deposited and electroplated Cu-Au bilayers can be used. The battery is then assembled layer by layer, bonded together with shellac glue, a natural and biocompatible alternative to synthetic glues. Chambers for the electrode pastes are cut out of untreated mycelium skin and glued onto the outer packaging layers on the metalized sides serving as current collectors. Pastes are filled into the chambers, and a separator frame and the liquid-filled mycelium skin separator are enclosed in between. Polarization curves of the assembled cells exhibit strictly linear behavior, and short-circuit currents up to ~50 mA are feasible (Fig. 3D). Using a vapor-deposited Cu-Au bilayer as cathode, current collector yields a discharge capacity of 3.8 mA hour cm^{-1} when discharged with a high current of 2 mA. We achieved high discharge capacities of up to 3.1 mA hour cm^{-1} using electroplated gold cathode current collectors at a high discharge current of 2 mA (Fig. 3E). Furthermore, with this simple assembling approach, multicell arrangements can easily be constructed, if higher voltages or capacities are needed.

Untethered MycelioTronic sensing circuit

Our mycelium battery concept allows autonomous operation of various electronics in a sustainable manner. Combining our metal trace fabrication approach with our mycelium batteries now enables standalone MycelioTronic circuits. We demonstrate an untethered mycelium sensor board, with a surface-mounted data communication module powered by an integrated mycelium battery and an embedded impedance sensor (Fig. 4A). The latter consists of two interdigitated electrodes with a length of 12 mm, a gap width of 400 μm, a trace width of 600 μm, and an overall width of 15 mm. We directly incorporate this sensor structure and two 15 mm by 15 mm electrodes for the mycelium battery in our circuit by laser ablation (fig. S12A) from copper-gold metalized mycelium skin. Collection and transmission of sensor data are handled by a commercial Bluetooth low-energy (BLE) module soldered to the respective connection pads in the circuit. To meet its power requirements (operating voltage of >1.9 V), we use two cells in series and assemble

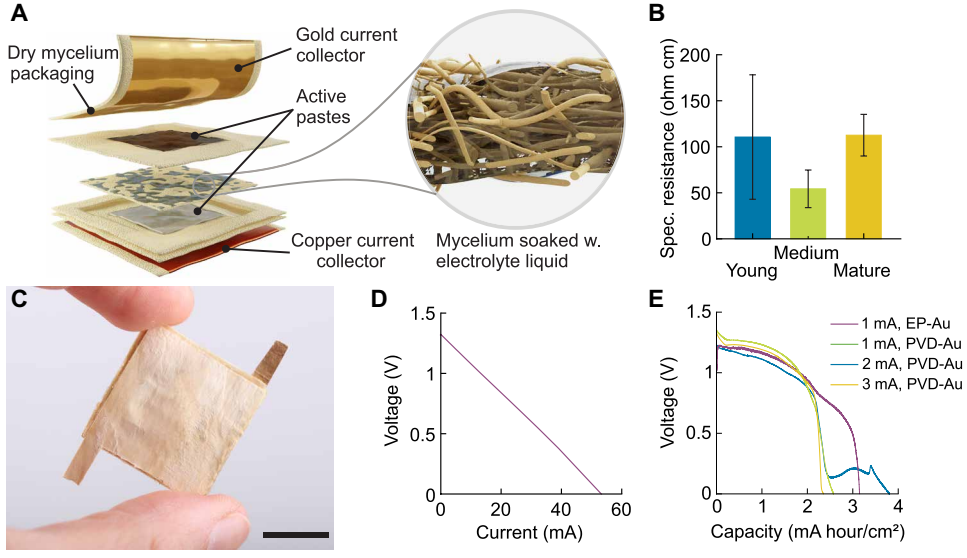

Fig. 3. Concept for mycelium batteries. (**A**) Explosion view of a mycelium zinc-carbon battery, using a mycelium separator soaked with electrolyte solution. (**B**) Specific resistance of young, medium, and mature electrolyte-filled mycelium. (**C**) Optical image of a sample battery. Scale bar, 1 cm. (**D**) Polarization curve of an assembled battery using a vapor-deposited gold cathode current collector. (**E**) Discharge of mycelium batteries with varying discharge current and both electroplated (EP-Au) and vapor-deposited (PVD-Au) cathode current collectors.

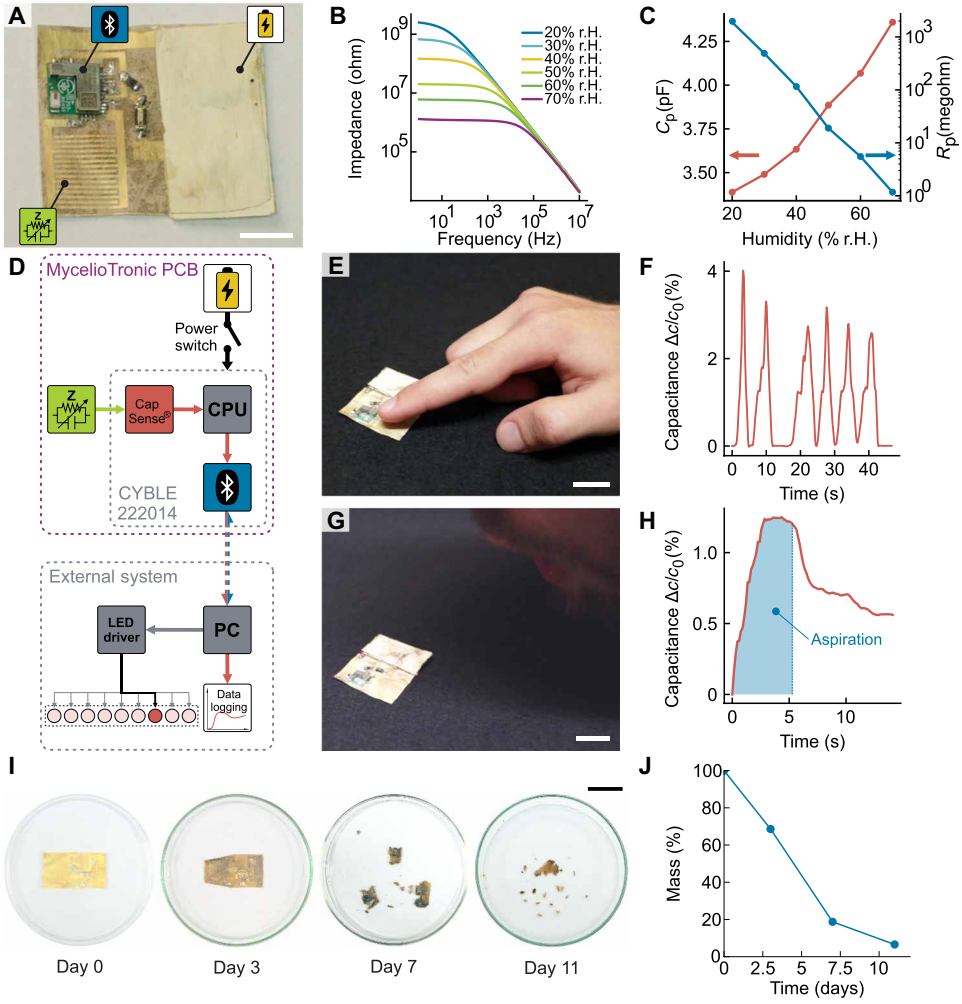

Fig. 4. Mycelium sensor board. (**A**) Photograph of a sensor board including a dual-cell mycelium battery, a Bluetooth module, and an impedance sensor with an interdigitated electrode structure. Scale bar, 1 cm. (**B**) Impedance response of the sensor highly depends on the relative humidity of the environment. (**C**) Fitted capacitance and resistance of the interdigitated sensor structure as function of frequency. (**D**) Block diagram of the sensor board generating and transferring data to an external PC during untethered experiments. (**E**) A finger approaching the sensor results in clear changes in sensor capacity. Scale bar, 2 cm. (**F**) Capacity response of the sensor to the repeatedly approaching finger in (E). (**G**) Aspiration onto the sensor board causes clearly detectable humidity changes. Scale bar, 2 cm. (**H**) Capacity response to the humidity changes on (G). (**I**) Aerobic disintegration of MycelioTronic PCB substrates occurs within 2 weeks in composting soil. Scale bar, 2 cm. (**J**) Mass percent of the decomposing PCB substrate depicted in (I) measured over 11 days.

the battery directly on the two integrated electrodes. Thus, the circuit substrate simultaneously functions as the bottom layer of the battery (fig. S12B). We first investigate the performance of our mycelium impedance sensor as humidity sensor within a controlled environment using a climate chamber (Fig. 4B). The relative humidity was gradually incremented by 10% relative humidity (r.H.) from 20 to 70% r.H. performing impedance spectra from 1 Hz to 10 MHz during stable climate conditions. Thereby, the impedance response can be modeled by a parallel capacitor-resistor circuit (fig. S13). The corresponding capacity increased around 29%, and the resistance decreased over three orders of magnitude to a resistance of 1.17 megohm at 70% r.H. (Fig. 4C). With this general high resistance and capacitance in the picofarad (pH) range, the sensor is suitable to be used with the built-in capacitance measurement system of the BLE module (Fig. 4D). Thereby, the sensor is periodically charged with a 2.2-nF capacitor to a reference voltage of 1.2 V (fig. S14) exhibiting only a slight leaking current of 0.5 μA at 70% r.H., negligible compared to the overall charging current of 138 μA. Combined with our mycelium battery, we demonstrate untethered humidity and proximity sensing with our circuit. The battery supplies a high operating current of approximately 2 mA under standard operation and approximately 13.5 mA during data transmission to the circuit. When an object like a finger approaches the sensor (Fig. 4E), its charging is altered as the object acts as a parasitic capacitance, resulting in distinct changes in sensor capacitance (Fig. 4F). In addition to proximity sensing, we also demonstrate the sensor's aspiration sensing capabilities (Fig. 4G). A short-term rise of humidity causes a clearly detectable change in capacity (Fig. 4H). After direct aspiration is terminated, the signal first decreases steeply, until a region of slower decrease caused by residual moisture adhering to the mycelium surface is observed. Thus,

we are able to conduct both proximity and humidity sensing entirely untethered and with an integrated sustainable power supply with our sustainable MycelioTronic design. We demonstrate the potential of finely structured circuits on mycelium skins powered by mycelium batteries. Our MycelioTronic approach therefore serves as a foundation for sustainable electronics with high functionality and variability. After the end of life of our circuit, reusable surface-mounted components are easily dissembled from the board using simple tools like a heat gun or solder iron, leaving solely the biodegradable substrate as waste product (fig. S15). The mycelium PCB disintegrates readily in composting soil after the removal of the conventional ICs (Fig. 4I). It loses 93.4% of its dry mass within 11 days (Fig. 4J). After this period, sample remnants are indistinguishable from the soil. Unprocessed mycelium skins disintegrate likewise down to 9.3% of their initial mass after 11 days (fig. S16). Furthermore, with our ability to use conventional IC elements, routes for improvement analogous to standard PCBs holds great promise. Implementation of vias through the skin constitutes only one of many promising routes for future improvements to the design and implementation of MycelioTronic circuits. Vias hold a vast potential toward multilayer PCBs with even higher complexity, closing the gap to conventional electronics in terms of sophistication. Traditionally, vias are realized by creating holes through the board and filling with a conductive material, connecting two or more layers. The soakability of the porous hyphen network of mycelium skins, however, allows for filling with conductive polymer suspensions, e.g., poly(3,4-ethylene dioxythiophene) polystyrene sulfonate (PEDOT:PSS) (fig. S17). This enables the fabrication of vias without the necessity of drilling or punching holes.

DISCUSSION

We here developed a new approach to fabricate sustainable electronics including power sources for untethered and standalone devices. We report methods for scalable growth of mycelium skins and fabrication of electronic traces on top these biodegradable substrates. We demonstrate PVD of gold and copper films combined with laser-assisted patterning and achieve high trace conductivities of $9.74 \pm 1.44 \times 10^4$ S cm^{-1}. Good flexibility of the substrate enables thin traces to be bent repeatedly 2000 times down to a bending radius of only 5 mm with only moderate increase in resistance. We additionally demonstrate the fabrication of mycelium-based batteries, substituting both the packaging and the separator of zinc-carbon cells with our sustainable mycelium skins that achieve capacities up to ~3.8 mA hour cm^{-2}. We use these batteries to power an untethered mycelium sensor board, able to measure, store, and transmit humidity and proximity sensing data. All the materials used can either be composted or be recycled. With these advances, biodegradable mycelium skins may emerge as a sustainable alternative materials class for a green electronic future.

MATERIALS AND METHODS

Materials

All chemicals were used as received without further purification. Ammonium chloride (NH_4Cl; Sigma-Aldrich) and zinc chloride ($ZnCl_2$; VWR, USA) were used as electrolyte solution. Zinc powder (Grillo-Werke AG, Germany), xanthan powder (Sigma-Aldrich), manganese(IV) oxide (MnO_2; Sigma-Aldrich), and acetylene carbon black (ABCR GmbH & Co KG, Germany) were used for the battery electrodes. Gold electrolyte solution (Conrad Electronic International GmbH & Co. KG) was used for galvanizing copper-plated mycelium. Shellac flakes (A.F. Suter & Co. Ltd.) were used to fabricate shellac glue. PEDOT:PSS (Clevios PH 1000, Heraeus) was used as conductive filler. Silver ink (Leitsilber 200, Ögussa) was used as conductive coating. Low-temperature solder (IND:282, Indium corporation) was used for soldering.

Mycelium skin growth and harvest procedure

One kilogram of dry beech wood shavings (Räucherspan.de Buche Typ 7) was thoroughly mixed with about 50 g of organic full-grain spelt flour (local grocery store) and 25 g of fine plaster ($CaSO_4$) dust (local construction market). This mixture together with 2 liters of water was boiled in a pressure cooker for at least 30 min for sterilization. The wet substrate was filled in sterilized polypropylene boxes to a height of 4 to 8 cm. After cooling down to room temperature with closed lid, about 500 g of beech wood–based inoculum (Tyroler Glückspilze Sägemehlbrut *G. lucidum* Sopron strain) was evenly distributed to all containers, manually ripped apart into small pieces, and mixed thoroughly under the substrate. As a separation grid, a strong polyethylene fly screen with square holes of 0.5 mm in width was cut to fit onto the surface of the substrate in the containers. After sterilization with boiling water and isopropanol, the fly screen patches are placed on the substrate, the lid are closed tightly to minimize gas exchange, and the boxes are stored in a dark space at approximately 25°C. After appropriate fungus growth, the separation grid was ripped off the solidified substrate together with the mycelium skin. The mycelium skin was peeled off carefully from the separation grid using a blade or a spatula. The wet skin was repeatedly placed between two paper towels and pressed gently to remove most of the water content. When the mycelium skin was dry to the touch, it was placed between two straight wood plates and left to completely dry while being forced flat.

TGA measurement

A crucible was filled with ~5 mg of mycelium skin, placed in a Mettler Toledo TGA, and flooded with pure O_2. The temperature was set to 50°C for 30 min and then increased with a rate of 0.166 K/s until 400°C.

SEM measurement

Scanning electron microscopy (SEM) measurements were performed using the Zeiss 1540 XB CrossBeam SEM (acceleration voltage, 5 keV). Before imaging, the samples were covered with ca. 10 nm of gold via thermal evaporation (pressure, ~3×10^{-6} mbar; deposition rate, 0.1 to 0.3 A s^{-1}) to increase surface conductivity and thus image quality.

Uniaxial tensile tests

Mycelium skin specimens were punched out with a dog bone–shaped punching tool based on ISO 527-2:2012(E) type 5A and tested with a Zwick Roell Z005 (100 N load cell).

Surface metallization (PVD)

Mycelium skin samples were metallized with a PVD system (Oerlikon Leybold Univex 350), using a vacuum pressure of less than 5×10^{-6} mbar. The deposition rates were 0.02 nm s^{-1} for chromium, 0.3 nm s^{-1} for copper, and 0.15 nm s^{-1} for gold.

Electroplating

Premetalized mycelium skin samples were submerged in a gold electrolyte solution (Conrad Electronic International GmbH & Co. KG) and connected to a power supply (Rohde & Schwarz München Typ NGM 70/05) with a fixed current supply of 100 mA. Hereby, a steel ring was used as the counter electrode.

Conductivity of metallized mycelium skins

The conductivity of a metallized trace on a mycelium skin was determined by measuring the resistance with a multimeter (Keithley 2110) in four-wire configuration. All mycelium samples are metallized with a chromium-copper-gold trilayer (3 nm of Cr, 400 nm of Cu, and 50 nm of Au), and the desired traces and pads were created by removing the negative by laser ablation with a fiber laser cutter (Trotec Speedy300 flexx). The conductivity σ was calculated as

$$\sigma = \frac{l}{R \cdot A} \quad (1)$$

where R is the measured resistance, A is the cross section (1 mm by 450 nm), and l is the length (10 mm) of the Cu-Au metal trace.

Cyclic bending

A mycelium sample with an engraved trace was placed on a 75-μm-thick polyimide foil (Kapton HN). The foil was clamped between two parallel poly(methyl methacrylate) plates, and the resistance was determined with a multimeter (Keithley 2110) in four-wire configuration. The distance between the two plates was adjusted periodically, and the bending radius is approximated as the halved distance between the two plates.

Folding experiment

A metallized mycelium sample (3 nm of Cr, 400 nm of Cu, and 50 nm of Au) was engraved to yield five parallel traces. The edge of a thin plastic plate was used to fix the sample around the desired folding edge following a second plate to fold the mycelium over the edge. After removing the first plate, the mycelium was compressed even further to ensure a hard edge. This process was repeated 12 times with alternating folding directions, and for each new fold, the previous folds are compressed as well. For every two new folds, the resistance was determined with a multimeter (Keightley 2110) in four-wire configuration.

Reshaping into helix structure

A metallized mycelium strip (3 nm of Cr, 400 nm of Cu, and 50 nm of Au) with a mounted LED was soaked with isopropanol and was helically wrapped around a 5-mm-thick glass tube. A thin gap in the metallic layer ensures the current flow through the LED, and a low-temperature solder paste (IND:282, Indium Corporation) was used to mount the LED. The wrapped mycelium was fixed on the endings of the strip with tape. As soon as the isopropanol was completely evaporated, the mycelium can be removed by sliding it over the glass tube. The mycelium stayed in the given helix structure without any additional process.

Impedance spectroscopy

Mycelium skin samples were soaked for 24 hours in electrolyte solution before testing. A custom-made measurement cell was used to determine the impedance between 1 and 10 MHz using an impedance analyzer (Novocontrol Alpha A Analyzer) with 1 mV of AC voltage applied. The bulk resistance was determined from the high-frequency plateau of the real part of the impedance. The conductivity and specific resistance were calculated using the bulk resistance and membrane geometry.

Battery fabrication

The anode paste was prepared by mixing 63.5 wt % zinc powder, 35 wt % electrolyte solution, and 1.5 wt % xanthan powder. The cathode paste was prepared by mixing 12 wt % manganese (IV) oxide and 12 wt % acetylene carbon black in 76 wt % electrolyte solution. For a single cell, the anode current collector is composed of a mycelium skin with a chromium-copper bilayer applied by vapor evaporation (3 nm of Cr and 900 nm of Cu). For the cathode current collector, gold was either deposited onto the same by electroplating with gold electrolyte solution and deposit time of 1 min or by subsequent PVD of a 50-nm gold layer. The mycelium was thoroughly rinsed and left to dry for 24 hours after electroplating. Chambers for the active anode and cathode pastes (1 cm by 1 cm) as well as a frame for the separator (1.5 cm by 1.5 cm) were cut out of plain, untreated mycelium skin sheets. The separator was soaked in electrolyte solution for at least 24 hours before assembly. One gram of shellac flakes was dissolved in 4 ml of ethanol and stirred for 20 hours to form an adhesive. The battery was constructed layer by layer, using shellac glue for adhesion of the mycelium skin layers to each other. For the two-cell configuration as used to power the circuit board, the anode current collector was, as well, made of gold-plated copper-mycelium skin.

Battery characterization

The characteristics of the batteries were recorded using a Keithley 2611A Source Measuring Unit connected to the battery current collectors.

Flexible PCB fabrication

The flexible PCB was based on a metallized mycelium skin with a chromium-copper-gold trilayer (3 nm of Cr, 400 nm of Cu, and 50 nm of Au). The traces and pads of the PCB were created by removing the negative by laser ablation with a fiber laser cutter (Trotec Speedy300 flexx). To avoid overheating and degradation of the mycelium skin over 250°C, all SMDs were soldered onto the pads with a low-temperature solder paste (IND:282, Indium Corporation). The core of the electronic system was a Bluetooth module (CYBLE-222014, Cypress Semiconductor Corp.). This module was connected to a Programmer/Debugger (Kitprog, Cypress) and flushed with a Bootloader program, enabling updating the module Over-The-Air via Bluetooth. The application of the module was programmed in PSoc Creator 4.2 and updated with the program CySmart 1.3 using the USB-dongle CY5677 CySmart BLE 4.2. To ensure a better connection to the PCB, short pieces of a copper wire were previously soldered onto the pads of the module to increase the size of the pads. An additional switch (CVS-01B, Copal Electronics) was included to cut off the power supply of the battery.

Humidity measurements

The mycelium sensor was placed in a climate chamber (C-40/350, CTS Clima Temperatur Systeme GmbH) and was read out with an impedance analyzer (Novocontrol Alpha A Analyzer) between 1 Hz and 10 MHz.

PEDOT:PSS soaking

Young mycelium skins were soaked with aqueous PEDOT:PSS solution either by submerging or by placing a droplet of PH1000 on the skin. Silver ink was used to contact the PEDOT:PSS-soaked mycelium.

Shellac coating of LED strip

Young metallized mycelium (3 nm of Cr, 400 nm of Cu, and 50 nm of Au) with three surface-mounted LEDs was brush-coated with a 1:4 shellac/ethanol mixture. The resulting shellac layer is an electrically insulating coating providing also mechanical protection. A second sample was coated with an airbrush, and the resulting surface structure was further analyzed by SEM.

Surface roughness measurement

Young mycelium skin of three different harvests were placed in a profilometer (Dektak 3), and the surface roughness R_{rms} was determined by calculating the root mean square average over a scanning length of 2 mm and averaging over all measured traces ($n = 9$).

Dielectric breakdown measurement

Young mycelium skins were positioned between two brass stamps connected to a high voltage supply (140-35000, FuG Elektonik GmbH). The voltage was continuously increased with 50 V s^{-1} until a breakdown/sharp voltage drop occurred.

Electrical property measurement

Double-sided metallized mycelium samples (3 nm of Cr and 500 nm of Cu) were engraved on both sides to form a plate capacitor with an area of 78.5 mm^2. The conducting electrodes are engraved in opposite directions and were connected with an impedance analyzer (Novocontrol Alpha A Analyzer). The impedance of the capacitor was determined between 10 and 1 MHz with 1 V of AC voltage applied. The relative permittivity ε_r, the conductivity σ, and the loss tangent δ are calculated from the complex impedance, taking into account the geometry of the electrodes.

Electrical heating measurement

A metallized mycelium sample (3 nm of Cr, 400 nm of Cu, and 50 nm of Au) was engraved to yield three parallel traces with a width of 2 mm. The traces were consecutively connected to a laboratory power supply (GPD-3303D, GW Instek) with step-wise increased current settings until failure. Simultaneously, a thermal infrared camera (325sc, FLIR) performs temperature measurements on the mycelium samples.

Biodecomposition measurement

Mycelium samples were mixed with properly operating aerobic composting inoculum and put into static composting vessels, purged with oxygen, and kept at a constant temperature of 58°C. For this purpose, the inoculum was first sorted to be free of large inert objects and to yield a homogeneous fine-grain mixture. Inoculum was then saturated with water and filled into the composting vessels along with mycelium samples. Vessels were sealed and purged with water-saturated air. Samples were filtered from the inoculum in intervals of 3 to 4 days, dried at 60°C, and weighed to yield the dry mass of samples. Photographs were taken, and mass loss was calculated with reference to the sample's original dry mass.

Statistical analysis

Sample size of trace conductivity and resistance measurements were $n = 5$ per type, data points being mean values and error bars indicating SD. Sample size of separator conductivity measurements was $n = 4$ per type, data points being mean values and error bars indicating SD. R_p and C_p values in Fig. 4C are fitted according to a parallel resistor-capacitor circuit model minimizing the least squared error of the impedance spectrum for each humidity setting using the Levenberg-Marquardt algorithm (fig. S7). All further measurement data are plotted as recorded.

SUPPLEMENTARY MATERIALS

Supplementary material for this article is available at https://science.org/doi/10.1126/sciadv.add7118

REFERENCES AND NOTES

1. A. Heiden, D. Preninger, L. Lehner, M. Baumgartner, M. Drack, E. Woritzka, D. Schiller, R. Gerstmayr, F. Hartmann, M. Kaltenbrunner, 3D printing of resilient biogels for omnidirectional and exteroceptive soft actuators. *Sci. Robot.* **7**, eabk2119 (2022).
2. Y. Khan, A. E. Ostfeld, C. M. Lochner, A. Pierre, A. C. Arias, Monitoring of vital signs with flexible and wearable medical devices. *Adv. Mater.* **28**, 4373–4395 (2016).
3. J. S. Heo, J. Eom, Y.-H. Kim, S. K. Park, Recent progress of textile-based wearable electronics: A comprehensive review of materials, devices, and applications. *Small* **14**, 1703034 (2018).
4. D. Hoornweg, P. Bhada-Tata, C. Kennedy, Environment: Waste production must peak this century. *Nature* **502**, 615–617 (2013).
5. M. Baumgartner, F. Hartmann, M. Drack, D. Preninger, D. Wirthl, R. Gerstmayr, L. Lehner, G. Mao, R. Pruckner, S. Demchyshyn, L. Reiter, M. Strobel, T. Stockinger, D. Schiller, S. Kimeswenger, F. Greibich, G. Buchberger, E. Bradt, S. Hild, S. Bauer, M. Kaltenbrunner, Resilient yet entirely degradable gelatin-based biogels for soft robots and electronics. *Nat. Mater.* **19**, 1102–1109 (2020).
6. W. Li, Q. Liu, Y. Zhang, C. Li, Z. He, W. C. H. Choy, P. J. Low, P. Sonar, A. K. K. Kyaw, Biodegradable materials and green processing for green electronics. *Adv. Mater.* **32**, 2001591 (2020).
7. T. Das, S. Tosoni, G. Pacchioni, Structural and electronic properties of bulk and ultrathin layers of V_2O_5 and MoO_3. *Comput. Mater. Sci.* **163**, 230–240 (2019).
8. T. Dinh, H.-P. Phan, T.-K. Nguyen, A. Qamar, A. R. Md Foisal, T. N. Viet, C.-D. Tran, Y. Zhu, N.-T. Nguyena, D. V. Dao, Environment-friendly carbon nanotube based flexible electronics for noninvasive and wearable healthcare. *J. Mater. Chem. C* **4**, 10061–10068 (2016).
9. C. Sun, X. Li, Z. Cai, F. Ge, Carbonized cotton fabric in situ electrodeposition polypyrrole as high-performance flexible electrode for wearable supercapacitor. *Electrochim. Acta* **296**, 617–626 (2019).
10. L. Xiang, H. Zhang, Y. Hu, L. M. Peng, Carbon nanotube-based flexible electronics. *J. Mater. Chem. C* **6**, 7714–7727 (2018).
11. S. Choi, H. Lee, R. Ghaffari, T. Hyeon, D.-H. Kim, Recent advances in flexible and stretchable bio-electronic devices integrated with nanomaterials. *Adv. Mater.* **28**, 4203–4218 (2016).
12. S. Li, K. Shu, C. Zhao, C. Wang, Z. Guo, G. Wallace, H. K. Liu, One-step synthesis of graphene/polypyrrole nanofiber composites as cathode material for a biocompatible zinc/polymer battery. *ACS Appl. Mater. Interfaces* **6**, 16679–16686 (2014).
13. L. H. Yamane, V. T. de Moraes, D. C. R. Espinosa, J. A. S. Tenório, Recycling of WEEE: Characterization of spent printed circuit boards from mobile phones and computers. *Waste Manag.* **31**, 2553–2558 (2011).
14. Y. Gao, Y. Zhang, X. Wang, K. Sim, J. Liu, J. Chen, X. Feng, H. Xu, C. Yu, Moisture-triggered physically transient electronics. *Sci. Adv.* **3**, e1701222 (2017).
15. L. Wang, K. Wang, Z. Lou, K. Jiang, G. Shen, Plant-based modular building blocks for "green" electronic skins. *Adv. Funct. Mater.* **28**, 1804510 (2018).
16. M. J. Tan, C. Owh, P. L. Chee, A. K. K. Kyaw, D. Kai, X. J. Loh, Biodegradable electronics: Cornerstone for sustainable electronics and transient applications. *J. Mater. Chem. C* **4**, 5531–5558 (2016).
17. A. C. Siegel, S. T. Phillips, M. D. Dickey, N. Lu, Z. Suo, G. M. Whitesides, Foldable printed circuit boards on paper substrates. *Adv. Funct. Mater.* **20**, 28–35 (2010).
18. J. Liu, C. Yang, H. Wu, Z. Lin, Z. Zhang, R. Wang, B. Li, F. Kang, L. Shi, C. P. Wong, Future paper based printed circuit boards for green electronics: Fabrication and life cycle assessment. *Energ. Environ. Sci.* **7**, 3674–3682 (2014).
19. Z. Fang, H. Zhu, W. Bao, C. Preston, Z. Liu, J. Dai, Y. Li, L. Hu, Highly transparent paper with tunable haze for green electronics. *Energ. Environ. Sci.* **7**, 3313–3319 (2014).
20. Y. H. Jung, T.-H. Chang, H. Zhang, C. Yao, Q. Zhen, V. W. Yang, H. Mi, M. Kim, S. J. Cho, D.-W. Park, H. Jiang, J. Lee, Y. Qiu, W. Zhou, Z. Cai, S. Gong, Z. Ma, High-performance

green flexible electronics based on biodegradable cellulose nanofibril paper. *Nat. Commun.* **6**, 7170 (2015).
21. Z. Liu, S. Nie, J. Luo, Y. Gao, X. Wang, Q. Wan, Flexible indium-tin-oxide homojunction thin-film transistors with two in-plane gates on cellulose-nanofiber-soaked papers. *Adv. Electron. Mater.* **5**, 1900235 (2019).
22. S. Nandy, S. Goswami, A. Marques, D. Gaspar, P. Grey, I. Cunha, D. Nunes, A. Pimentel, R. Igreja, P. Barquinha, L. Pereira, E. Fortunato, R. Martins, Cellulose: A contribution for the zero e-waste challenge. *Adv. Mater. Technol.* **6**, 2000994 (2021).
23. M. Haneef, L. Ceseracciu, C. Canale, I. S. Bayer, J. A. Heredia-Guerrero, A. Athanassiou, Advanced materials from fungal mycelium: Fabrication and tuning of physical properties. *Sci. Rep.* **7**, 41292 (2017).
24. I. Kuznetsova, B. Zaitsev, L. Krasnopolskaya, A. Teplykh, A. Semyonov, A. Avtonomova, M. Ziangirova, A. Smirnov, V. Kolesov, Influence of humidity on the acoustic properties of mushroom mycelium films used as sensitive layers for acoustic humidity sensors. *Sensors (Switzerland)* **20**, 2711 (2020).
25. M. R. Islam, G. Tudryn, R. Bucinell, L. Schadler, R. C. Picu, Morphology and mechanics of fungal mycelium. *Sci. Rep.* **7**, 13070 (2017).
26. F. V. W. Appels, J. G. van den Brandhof, J. Dijksterhuis, G. W. de Kort, H. A. B. Wösten, Fungal mycelium classified in different material families based on glycerol treatment. *Commun. Biol.* **3**, 334 (2020).
27. A. Van Wylick, E. Elsacker, L. L. Yap, E. Peeters, L. de Laet, Mycelium composites and their biodegradability: An exploration on the disintegration of mycelium-based materials in soil. *Bio Based Build. Mater.* **1**, 652–659 (2022).
28. E. S. Lazaro Vasquez, K. Vega, From plastic to biomaterials: Prototyping DIY electronics with mycelium, in *UbiComp/ISWC 2019- - Adjunct Proceedings of the 2019 ACM International Joint Conference on Pervasive and Ubiquitous Computing and Proceedings of the 2019 ACM International Symposium on Wearable Computers* (Association for Computing Machinery, 2019), pp. 308–311, doi:10.1145/3341162.3343808.
29. A. Adamatzky, A. Gandia, A. Chiolerio, Towards fungal sensing skin. *Fungal Biol. Biotechnol.* **8**, 6 (2021).
30. M. Jones, A. Mautner, S. Luenco, A. Bismarck, S. John, Engineered mycelium composite construction materials from fungal biorefineries: A critical review. *Mater. Des.* **187**, 108397 (2020).
31. E. Elsacker, E. Peeters, L. De Laet, Mycelium-based materials at the dawn of the anthropocene, in *Structures and Architecture: Bridging the Gap and Crossing Borders—Proceedings fo the Fourth International Conference on Structures and Architectrue ICSA 2019* (CRC Press, 2019), pp. 1083–1090, uresdoi:10.1201/9781315229126-129.
32. V. Meyer, E. Y. Basenko, J. P. Benz, G. H. Braus, M. X. Caddick, M. Csukai, R. P. de Vries, D. Endy, J. C. Frisvad, N. Gunde-Cimerman, T. Haarmann, Y. Hadar, K. Hansen, R. I. Johnson, N. P. Keller, N. Kraševec, U. H. Mortensen, R. Perez, A. F. J. Ram, E. Record, P. Ross, V. Shapaval, C. Steiniger, H. van den Brink, J. van Munster, O. Yarden, H. A. B. Wösten, Growing a circular economy with fungal biotechnology: A white paper. *Fungal Biol. Biotechnol.* **7**, 5 (2020).
33. M. Jones, A. Gandia, S. John, A. Bismarck, Leather-like material biofabrication using fungi. *Nat. Sustain.* **4**, 9–16 (2021).
34. H. Aouani, J. Wenger, D. Gerard, H. Rigneault, E. Devaux, T. W. Ebbesen, F. Mahdavi, T. Xu, S. Blair, Crucial role of the adhesion layer on the plasmonic fluorescence enhancement. *ACS Nano* **3**, 2043–2048 (2009).
35. D. Tobjörk, R. Österbacka, Paper electronics. *Adv. Mater.* **23**, 1935–1961 (2011).
36. B.-J. Kim, H. Shin, S.-Y. Jung, Y. Cho, O. Kraft, I.-S. Choi, Y.-C. Joo, Crack nucleation during mechanical fatigue in thin metal films on flexible substrates. *Acta Mater.* **61**, 3473–3481 (2013).
37. J. Wang, L. Emmerich, J. Wu, P. Vana, K. Zhang, Hydroplastic polymers as eco-friendly hydrosetting plastics. *Nat. Sustain.* **4**, 877–883 (2021).
38. D. Larcher, J. M. Tarascon, Towards greener and more sustainable batteries for electrical energy storage. *Nat. Chem.* **7**, 19–29 (2015).
39. P. Arora, Z. Zhang, Battery separators. *Chem. Rev.* **104**, 4419–4462 (2004).
40. S. Leijonmarck, A. Cornell, G. Lindbergh, L. Wågberg, Single-paper flexible Li-ion battery cells through a paper-making process based on nano-fibrillated cellulose. *J. Mater. Chem. A* **1**, 4671–4677 (2013).
41. D. Grimm, H. A. B. Wösten, Mushroom cultivation in the circular economy. *Appl. Microbiol. Biotechnol.* **102**, 7795–7803 (2018).
42. D. Danninger, F. Hartmann, W. Paschinger, R. Pruckner, R. Schwödiauer, S. Demchyshyn, A. Bismarck, S. Bauer, M. Kaltenbrunner, Stretchable polymerized high internal phase emulsion separators for high performance soft batteries. *Adv. Energy Mater.* **10**, 2000467 (2020).

Acknowledgments: We thank S. Demchyshyn for support with SEM measurements. **Funding:** This work was supported by an ERC Starting Grant "GEL-SYS" 757931 (to M.K.) and the Austrian Research Promotion Agency GmbH (FFG) "Myco-Insulation" FO999891082 (to M.K.). **Author contributions:** Conceptualization: R.P., D.D., R.K., and M.K. Methodology: R.P., D.D., R.K., and M.K. Investigation: R.P., D.D., L.H., and R.K. Visualization: R.P. and D.D. Supervision: R.K. and M.K. Writing—original draft: D.D., R.P., and R.K. Writing—review and editing: D.D., R.P., R.K., and M.K. **Competing interests:** The authors declare that they have no competing interests. **Data and materials availability:** All data needed to evaluate the conclusions in the paper are present in the paper and/or the Supplementary Materials. Supplementary information is available online.

Submitted 29 June 2022
Accepted 26 September 2022
Published 11 November 2022
10.1126/sciadv.add7118